rall–Jencks energy diagrams (arrow 2 in Figure 2).[11,19] A reaction coordinate with a large component of hydron transfer can give rise to a Hammond effect that can result in a decrease in the extent of hydron transfer.[11,19,54] A reaction coordinate with a large component of hydron transfer is expected here, because the small halogen leaving group effects mean that the E2 transition states in these reactions are very carbanion-like and are near the top edge of the energy diagram in Figure 2. In contrast to these results, the Brönsted $\beta$ values of 0.50[55] and 0.54, and 0.50[55] and 0.49 for the elimination reactions of 2-(2,4-dinitrophenyl)ethyl[19] and 2-(2,4,6-trinitrophenyl)ethyl fluoride, and 2-(2,4-dinitrophenyl)ethyl[19] and 2-(2,4,6-trinitrophenyl)ethyl chlorides, respectively, are consistent with a zero $p_{xy}$ interaction coefficient[56] that, along with the small $k_F:k_{Cl}$ ratio and the small dependence of this ratio on the $\beta$-aryl substituent cited above, may signify a change to the $E1cB_{irr}$ mechanism for the reactions of these substrates.

**Acknowledgment**. We are grateful to Professor W. P. Jencks for helpful comments.

(54) Thornton, E. R.; Winey, D. A. *J. Am. Chem. Soc.* **1977**, *97*, 3102.

(55) On further inspection of the data, the previously reported Brönsted $\beta$ values for the 2-(2,4-dinitrophenyl)ethyl fluoride, chloride, bromide, and iodide have been corrected to values of 0.50, 0.50, 0.46, and 0.42, respectively (compared to the previously reported values of 0.54, 0.54, 0.46, and 0.42).

(56) On its own, a zero $p_{xy}$ coefficient does not establish the $E1cB_{irr}$ mechanism because it is not clear why this coefficient would be smaller for an $E1cB_{irr}$ than an E2 mechanism.

# Conformation of the Glycolipid Globoside Head Group in Various Solvents and in the Micelle-Bound State

**Leszek Poppe,[†,§] Claus-Wilhelm von der Lieth,[‡] and Janusz Dabrowski*[,†]**

*Contribution from the Max-Planck-Institut für Medizinische Forschung, D-6900 Heidelberg, Germany, and Deutsches Krebsforschungszentrum, D-6900 Heidelberg, Germany.*
*Received September 27, 1989*

**Abstract:** The three-dimensional (3D) structure of the oligosaccharide part of the globotetraosylceramide (globoside), GalNAc$\beta$1-3Gal$\alpha$1-4Gal$\beta$1-4Glc$\beta$1-1Cer, was modeled in $Me_2SO$ and $Me_2NCHO$ solutions with use of a distance mapping procedure, which involved NOE contacts between the amido, hydroxy, and C-linked protons. The oligosaccharide chain showed a pronounced flexibility of each of the glycosidic linkages, while preserving a global "L" shape. A similar conformation was found for globoside anchored in mixed dodecylphosphocholin micelles in $D_2O$ solution, where it experiences a fast internal rotation on a time scale of 0.4 ns. It was concluded that the hard-sphere exo-anomeric (HSEA) model applied elsewhere did not predict correctly the 3D structure of globoside, while molecular mechanics calculations, used extensively in the present work, approach more closely the true oligosaccharide conformations.

The biological role of glycan moieties of glycolipids[1a] and glycoproteins[1b] is well-documented, and a great number of observations suggest that conformation of oligosaccharide chains is responsible for their specific interaction with a variety of receptors.[1c-e] NMR studies of solution conformation of biomolecules of any class are mainly based on the proton–proton distance information gained from the quantitative evaluation of NOE data.[2a] However, in contrast to proteins, oligopeptides, and nucleic acids, which usually display a sufficient number of NOE connectivities to be used (in combination with energy minimum calculations) in the modeling of well-founded three-dimensional structures,[2b,c] oligosaccharides show very few structurally relevant NOE contacts so that the conformational analysis is slanted toward theoretical calculations. At the same time, systematic scanning of the conformational space of oligosaccharides by means of quantum mechanical[3a] and molecular mechanics[3b-f] calculations does not presently extend beyond disaccharides because of the excessive computational time required. The energy minimization of more complex systems is usually trapped in local minima, which can be very different from the global one. Restarting the minimization process with different, randomly chosen geometries often yields a number of energetically similar, yet different conformations whose relative importance with respect to one another cannot be assessed properly owing to the limited accuracy of empirical energy calculations. These computational difficulties can be skipped if one uses a simplified or "smoothed" potential energy hypersurface as in the HSEA (hard-sphere exo-anomeric) model where only van der Waals (vdW) interactions and the exo-anomeric effect are taken into account.[4a-c] Recently, however, this method has been subjected to criticism[3b] (cf. a discussion reviewed in ref 3b); also the present study shows that the torsional freedom for glycosidic bonds is far more pronounced than predicted by the HSEA model.

In a preliminary communication we have shown that many more structurally important NOE contacts can be observed in rotating

* Author to whom correspondence should be addressed.
† Max-Planck-Institut.
§ Present address: Complex Carbohydrate Research Center, The University of Georgia, Athens, GA 30602.
‡ Deutsches Krebsforschungszentrum.

(1) (a) Hakomori, S. I. *Sci. Am.* **1986**, *254*, 32-41. (b) Feizi, T. *Nature* **1985**, *314*, 53-57. (c) Hounsell, E. F. *Chem. Soc. Rev.* **1987**, *16*, 161-185. (d) Bock, K. *Pure Appl. Chem.* **1987**, *59*, 1447-1456. (e) Karlsson K. A. *Pure Appl. Chem.* **1987**, *59*, 1447-1448.

(2) (a) Neuhaus, D.; Williamson, M. P. *The Nuclear Overhauser Effect in Structural and Conformational Analysis*; VCH Publishers: New York, 1989. (b) Wüthrich, K. *NMR of Proteins and Nucleic Acids*; John Wiley & Sons: New York, 1986. (c) Pepermans, H.; Tourwe, D.; van Binst, G.; Boelens, R.; Scheek, R. M.; van Gunsteren, W. F.; Kaptein, R. *Biopolymers* **1988**, *27*, 323-338.

(3) (a) Yadav, J. S.; Luger, P. *Carbohydr. Res.* **1983**, *119*, 57-73. (b) Tvaroska, I.; Perez, S. *Carbohydr. Res.* **1986**, *149*, 389-410. (c) Rasmussen, K. In *Molecular Structure and Dynamics*; Balaban, M., Ed.; International Science Services: Philadelphia, 1980; pp 171-210. (d) Tran, V.; Buleou, A.; Perez, S. *Biopolymers* **1989**, *28*, 679-690. (e) French, A. D. *Biopolymers* **1988**, *27*, 1519-1525. (f) Ha, S. N.; Madsen, L. J.; Brady, J. W. *Biopolymers* **1988**, *27*, 1927-1952.

(4) (a) Lemieux, R. U.; Bock, K.; Delbaere, L. T. J.; Koto, S.; Rao, V. S. *Can. J. Chem.* **1980**, *58*, 631. (b) Bock, K. *Pure Appl. Chem.* **1983**, *55*, 605-622. (c) Thogersen, M.; Lemieux, R. U.; Bock, K.; Meyer, B. *Can. J. Chem.* **1982**, *60*, 44-57.

0002-7863/90/1512-7762$02.50/0 

Table I. Chemical Shifts for Globoside in $Me_2NCHO$-$d_7$ at 310 K and in $D_2O$/DPC Solution at 303 K (Italicized)

| residue | | 1 | 2 | 3 | 4 | 5 | 6*R* | 6*S* |
|---|---|---|---|---|---|---|---|---|
| GalNAcβ-IV | CH | 4.69 | 3.87 | 3.59 | 3.83 | 3.47 | 3.73 | 3.67 |
| | | *4.69* | *4.01* | *3.81* | *4.01* | *3.73* | *3.86* | *3.79* |
| | OH | | 7.80[a] | 5.13 | 4.56 | | 4.62 | |
| Galα-III | CH | 4.95 | 3.98 | 3.81 | 4.15 | 4.26 | 3.64 | 3.66 |
| | | *4.97* | *3.94* | *4.01* | *4.30* | *4.43* | *3.73* | *3.74* |
| | OH | | 4.92 | | 4.45 | | 4.48 | |
| Galβ-II | CH | 4.43 | 3.57 | 3.57 | 4.15 | 3.75 | 3.89 | 3.76 |
| | | *4.56* | *3.64* | *3.80* | *4.10* | *3.85* | *3.97* | *3.89* |
| | OH | | 5.27 | 4.54 | | | 4.90 | |
| Glcβ-I | CH | 4.31 | 3.19 | 3.48 | 3.47 | 3.43 | 3.80 | 3.88 |
| | | *4.50* | *3.40* | *[3.71* | | *3.65]*[b] | *3.83* | *4.04* |
| | OH | | 5.24 | 4.64 | | | 4.62 | |

[a] NH. [b] Strongly coupled.

frame spectra of samples with unexchanged hydroxyl and amido groups.[5] In this way the experimental basis for a verification of theoretically calculated conformation(s) can be greatly extended. Here we analyze the globoside head group structure in quantitative terms.

Energy minimization was performed with use of the molecular mechanics MM2(85) program,[6] with starting structures obtained from a purely geometric analysis based on experimentally derived interatomic distances. Our approach differs substantially from that applied in the investigation of deuterium-exchanged globoside in $Me_2SO$ solution where NOE data were fitted by one- and two-state models based on HSEA and molecular mechanics calculations, including additional pseudoenergy terms derived from experimentally obtained interproton distances.[7a,b]

The conformational analysis presented in the following sections is essentially based on rotating frame NOE (CAMELSPIN[8a] or ROESY[8b]) measurements for native globoside dissolved in $Me_2SO$ or $Me_2NCHO$. The conformational analysis of micelle-bound globoside in $D_2O$ follows this. Measurements of selective and nonselective initial relaxation rates at two magnetic fields (500 and 360 MHz) gave some insight into the structure and dynamics of the intact glycolipid in this more natural environment.

## Materials and Methods

Globoside (5 mg), purchased from BioCarb (Lund, Sweden), was dried in high vacuum and dissolved in 0.4 mL of $Me_2SO$-$d_6$ or $Me_2NCHO$-$d_7$. Dodecylphosphocholine-$d_{38}$ (DPC) was obtained from Merck, Sharp & Dohme. The sample investigated in $D_2O$ (50 mM phosphate buffer, pD ~ 7) was 4 mM in globoside and 0.2 M in detergent. The solutions were degassed and sealed under Argon.

**NMR Measurements.** NMR spectra were obtained at frequencies of 500 and 360 MHz with Bruker AM-500 and AM-360 spectrometers equipped with Aspect 3000 computers, process controllers, array processors, and a selective excitation unit. Chemical shifts were referenced to $Me_4Si$ either directly (for micelles) or indirectly by setting the $^1H$ signal of residual $Me_2SO$-$d_5$ or $Me_2NCHO$-$d_6$ at 2.50 or 8.01 ppm, respectively. Spectral assignments in $Me_2SO$ have been reported earlier,[5] and the data for solutions in $Me_2NCHO$ and $D_2O$ are presented in Table I.

Two-dimensional (2D) ROESY and NOESY spectra were recorded in the phase-sensitive mode with use of the TPPI method at 500 MHz. A Hahn-echo pulse sequence was applied before acquisition[9] and the receiver phase adjusted to the absorption mode[10] in order to avoid baseline distortion. For ROESY experiments the pulse sequence proposed by Rance[11] was used, the mixing time (ca. 200 ms) being composed of a train of short (ca. 20°) pulses[12] sandwiched by two 170° pulses[13] and by two z filters. The rf carrier frequency was placed about 1.5 kHz downfield relative to the center of proton resonances during the spin-lock time and at the center during evolution and acquisition. The effective field for spin-locking was 2–2.5 kHz. A total of 512 free induction decays (FIDs), 64 scans each, were accumulated with $t_1$ and $t_2$ acquisition times of 0.128 and 0.256 s, respectively; the relaxation delay was 1.5 s. The 2D ROESY spectra for the $Me_2SO$ solution were recorded at 291, 289, 315, and 333 K and those for the $Me_2NCHO$ solution at 279, 288, and 310 K. The $\omega_1$ decoupled selective 2D ROESY experiment was performed according to the pulse sequence devised by Brüschweiler et al.[14] The selective 90° and 180° Gaussian pulses (truncated at a 2% level) were of 8.9- and 9.2-ms duration. A total of 128 FIDs, 128 scans each, were accumulated with $t_1$ and $t_2$ acquisition times of 0.426 and 0.341 s. The 2D ROESY spectra for the aqueous solution were measured at 303 K with 50 and 100 ms mixing times, using the pulse sequence described above. The 2D NOESY spectra were measured at the same temperature with 50, 100, and 150 ms mixing times. All 2D time domain spectra were zero filled, multiplied by a squared cosine bell, or a Lorentzian–Gaussian function and transformed to give a final resolution of 1.95 Hz/pt in $\omega_2$ and 3.9 Hz/pt in $\omega_1$ for nonselective experiments and 1.47 Hz/pt in $\omega_2$ and 1.17 Hz/pt in $\omega_1$ for a selective experiment. Peak volumes were calculated by using the 2D integration routine contained in Bruker software. The cross-peak volumes were correted for offset effects as described in the Theory section. For significant Hartmann–Hahn effects the volumes were corrected according to the equation $V_{m,n}(\text{corr}) = V_{m,n}(\text{obs})/(1 - \eta^2)(1 + \eta)$, where $V_{m,n}(\text{corr})$ are the corrected cross-peak volumes for coupled spins m and n, and $\eta$ is the transfer coefficient equal to $0.5s_{mn}^2$ as described in the Theory section. The exchange contribution to cross-peak volumes was insignificant at low temperatures and no efforts were made to treat it quantitatively. The $r^*$ distances were calculated by using the expression $r_{kl} = r_{0ij}(V_{0ij}/V_{kl})^{1/6}$, where $V_{0ij}$ and $r_{0ij}$ are the cross-peak volume and distance for the reference interaction. The distances listed in Table IV are average values obtained from different experiments and different calibrations. The estimated errors are ≤0.1 Å for distances ≤2.5 Å, ≤0.2 Å for distances ≤3.2 Å, ≤0.3 Å for distances ≤3.7 Å, and ≤0.5 Å for distances ≤4.5 Å. One-dimensional (1D) transient ROESY and NOESY spectra were recorded with direct subtraction of the reference FID every eight scans, with a total accumulation of 800 scans per spectrum; the relaxation delay was 1.5 s and the acquisition time was 1 s. For DPC-dissolved globoside the mixing time was varied in the 30–150-ms range. The cross-relaxation rates were obtained with a 15% precision from the initial builtup of signal integrals in 1D and cross-peak volumes in 2D NOESY and ROESY spectra.

The selective and nonselective relaxation experiments were measured at 500 and 360 MHz with 15 values for the waiting time $\tau$, between a selective or nonselective 180° pulse and a 90° read pulse, within the range of 5–100 ms for selective and 5–200 ms for nonselective inversion pulses. Relaxation delay was 12 s and 16 scans were accumulated for each $\tau$ value. Before Fourier transformation the FIDs were multiplied exponentially (LB = 2 Hz) and zero filled. The relaxation rates were obtained from linear regression analysis of the measured signal intensities. The selective 180° pulses were Gaussian or DANTE pulses with a duration of 10 ms.

One-dimensional "total correlation spectroscopy" (TOCSY,[15a] HOHAHA[15b]) experiments were done as described by Subramanian and Bax[15b] with variable mixing time during accumulation and selective irradiation of a OH6 proton.[5] The pulse sequence for the 1D COSY experiment with a chemical shift selective filter was that proposed by Hall and Norwood.[16] For the aqueous solution the frequency of the filter, having a bandwidth of 5 Hz, was adjusted to the resonance of one of the H5, H6, or H6′ protons. The theoretical spectra for the H5H6H6′OH6 spin systems were simulated by using the Bruker PANIC program. An error of about 0.7 Hz in the vicinal coupling constant introduces a maximum bias of 0.15 on calculated populations of hydroxymethyl groups.

**Theoretical and Computational Aspects.** The interproton distances can be obtained by comparing the magnitudes of the cross-relaxation rates for two different proton pairs

$$r_{kl} = r_{0ij}(\sigma_{0ij}/\sigma_{kl})^{1/6} \quad (1)$$

where $r_{kl}$ is unknown and $r_{0ij}$ is the known, calibration distance; $\sigma$ is the laboratory ($\sigma_\parallel$) or rotating frame ($\sigma_\perp$) cross-relaxation rate, measured

(5) Dabrowski, J.; Poppe, L. *J. Am. Chem. Soc.* **1989**, *111*, 629–630.
(6) Burkert, V.; Allinger, N. L. *Molecular Mechanics*; American Chemical Society: Washington, DC, 1982; ACS Monogr. 177.
(7) (a) Scarsdale, J. N.; Yu, R. K.; Prestegard, J. H. *J. Am. Chem. Soc.* **1986**, *108*, 6778–6784. (b) Scarsdale, J. N.; Ram, P.; Prestegard, J. H.; Yu, R. K. *J. Comput. Chem.* **1988**, *9*, 133–147.
(8) (a) Bothner-By, A. A.; Stephens, R. L.; Lee, J.; Warren, Ch. D.; Jeanloz, R. W. *J. Am. Chem. Soc.* **1984**, *106*, 811–813. (b) Bax, A.; Davis, D. G. *J. Magn. Reson.* **1985**, *64*, 533–535.
(9) Davis, D. G. *J. Magn. Reson.* **1989**, *81*, 603–607.
(10) Marion, D.; Bax, A. *J. Magn. Reson.* **1988**, *79*, 352–356.
(11) Rance, M. *J. Magn. Reson.* **1987**, *74*, 557–564.
(12) Kessler, H.; Griesinger, C.; Kerssebaum, R.; Wagner, K.; Ernst, R. R. *J. Am. Chem. Soc.* **1987**, *109*, 607–609.
(13) Dezheng, Z.; Toshimichi, F.; Nagayama, K. *J. Magn. Reson.* **1989**, *81*, 628–630.
(14) Brüschweiler, R.; Griesinger, C.; Sorensen, O. W.; Ernst, R. R. *J. Magn. Reson.* **1988**, *78*, 178–185.
(15) (a) Braunschweiler, L.; Ernst, R. R. *J. Magn. Reson.* **1983**, *53*, 521–528. (b) Subramanian, S.; Bax, A. *J. Magn. Reson.* **1987**, *71*, 325–330.
(16) Hall, L. D.; Norwood, T. J. *J. Magn. Reson.* **1988**, *76*, 548–554.

from transient 1D or 2D NOESY[17] or ROESY[18,19] experiments. Isotropic motion of the molecule is assumed. For globoside, a molecule of medium size, the correlation time for isotropic tumbling, estimated from relaxation data, is in the range 0.4–1 ns, depending on temperature, so that the sensitivity of ROESY experiments is greater than corresponding NOESY experiments.[20] Moreover, the rotating frame cross-relaxation rates are significantly less dependent in this range on motional anisotropy than their laboratory frame counterparts,[20] hence one can expect that "ROE distances" estimated with eq 1 are more reliable than "NOE distances" so determined.

In a 2D ROESY spectrum relaxation can be related to cross-peak volumes[21]

$$a_{kl} = (\sin \theta_k)(\sin \theta_l)(e^{L\tau m})_{kl} M_{10} \quad (2)$$

where L is the mixing operator, $\tau_m$ is the mixing time, and $M_{10}$ is the equilibrium magnetization of spin 1. The trigonometrical terms arise from different offsets $\Omega_k$ and $\Omega_l$ from the carrier frequency;[21,22] $\theta_k = \arctan(\nu/\Omega_k)$, $\nu$ being the spin-lock field strength, usually of the order 2–3.5 kHz. For sufficiently short mixing times, so that $L_{kl}\tau_m \ll 1$, the $a_{kl}$ cross-peak volume is directly proportional to $L_{kl}$. Hartmann–Hahn magnetization transfer (direct and NOE-relayed via a third spin m) must be taken into account, however, and chemical exchange may also contribute to $L_{kl}$, hence[21]

$$L_{kl}\tau_m \approx -\sigma_{kl}\tau_m + (\cos(\theta_k - \theta_l))k_{kl}\tau_m + 0.5(s_{kl}^2 - \sigma_{km}\tau_m s_{ml}^2) \quad (3)$$

where $\sigma_{kl} = (\sin \theta_k)(\sin \theta_l)\sigma_{\perp kl} + (\cos \theta_k)(\cos \theta_l)\sigma_{\parallel kl}$ is the cross-relaxation rate in the rotating frame and $\sigma_{km}$ is defined similarly. The longitudinal contribution, $\sigma_{\parallel kl}$, to the rotating frame cross-relaxation rate is negligible, at least for all the cases studied here, and can be safely omitted. The last term in eq 3 is the direct and NOE-relayed Hartmann–Hahn magnetization transfer:

$$s_{kl}^2 = (1 + \cos(\theta_k - \theta_l))^2 J_{kl}^2 / ((1 + \cos(\theta_k - \theta_l))^2 J_{kl}^2 + 4(\nu_k - \nu_l)^2)$$

where $\nu_k$ and $\nu_l$ are the effective fields for spins k and l, e.g., $\nu_k = (\nu^2 + \Omega_k^2)^{1/2}$, and $J$ is the coupling constant. The Hartmann–Hahn contribution is the most severe drawback to the use of this method; it is possible, however, to decrease this contribution drastically by choosing the appropriate offset for the carrier frequency during the spin-locking pulse sequence.[21] The cross-peak volume is further attenuated by the factor $1 - 0.5\sum s_{ij}^2$ due to the relayed Hartmann–Hahn magnetization transfer to the coupled spins.[21]

In the limit of slow molecular tumbling, the chemical exchange contribution, $k_{kl}$, has the opposite sign to that originating from $\sigma_\perp$ and the same as that from $\sigma_\parallel$, hence it can be eliminated in the easily realizable case of $\theta_k - \theta_l \approx 0$ by recording NOESY and ROESY spectra under the same conditions and adding appropriately scaled cross-peak volumes obtained in these two experiments. In the fast-tumbling limit this procedure is of little value because of cancellation of $\sigma_\perp$ and $\sigma_\parallel$ in this case.

In the absence of chemical exchange, and for short mixing times, one can replace cross-relaxation rates in eq 1 by scaled cross-peak volumes, according to eqs 2 and 3. The scaling factor $\sin \theta_k \sin \theta_l$ from eq 2 can be elimiated by a special pulse sequence.[13] In common practice, for reasons of higher sensitivity, ROESY spectra are recorded with longer mixing times (ca. 200 ms), the result being that although spin diffusion is still negligible, the leakage relaxation causes a non-uniform decrease in cross-peak volumes. The way to overcome this bias is to scale the cross-peak volume with use of a weighted sum of the corresponding (k,l) diagonal peak volumes.[23] Unfortunately, this procedure is rarely possible with crowded spectra. The unfavorable consequence of ignoring leakage relaxation is the tendency to underestimate short distances and to overestimate long distances. Cross-relaxation rates increase almost linearly with increasing solvent viscosity, and for unfavorable spin geometries, spin diffusion or rather the "three spin effect" may considerably influence cross-peak volumes.[24a,b] This is most pronounced for weak interactions, and, in consequence, the longer distances would again be overestimated, completely the opposite to the NOESY derived distances in the short mixing time regime.[25] An easy way to control this type of artefact is to record ROESY spectra at different temperatures.

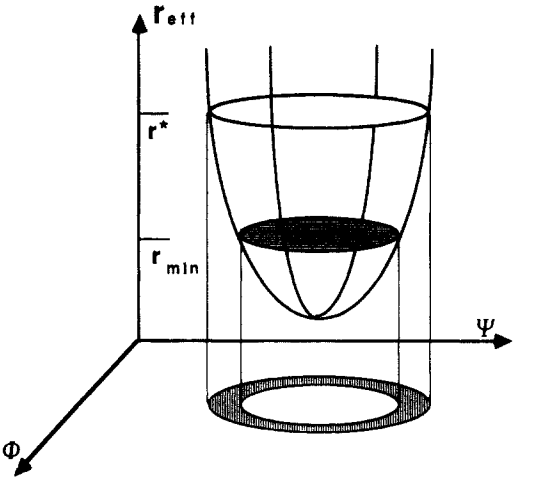


**Figure 1.** Simplified scheme of the distance mapping procedure: $r$(eff) is the effective distance calculated with eq 4 for pendent protons, $r^*$ is the "NOE distance" cited in Table IV, and $r_{min}$ corresponds to the minimum separation, calculated on the basis of vdW contacts.

The analysis of interatomic distances, obtained from NOE measurements, in terms of glycosidic bond conformations was described in detail in the previous paper;[26] here we stress the main points again.

For an oligosacharide chain, which can adopt a variety of backbone conformations, each corresponding to a unique set of glycosidic bond angles, the interatomic distances calculated from cross-relaxation data are "virtual",[27] if the interconversion rate is fast on the NMR time scale. Consequently, for each atom pair showing NOE connectivity, there must be at least one pair of true $H_k\cdots H_l$ distances, one of them being larger and the other one smaller than the measured "NOE distance" $r_{kl}$. Since it is impossible to define the upper distance limit from relaxation data for these two nuclei (except for rough estimations based, for example, on the uniform averaging model[28]), we intentionally neglect the conformers with longer $H_k\cdots H_l$ distances and only analyze situations in which $r_{kl} < r^*_{kl}$, where at least one conformation can be found with confidence. The $r^*_{kl}$ value is thus considered as the upper limit and the sum of vdW radii as a lower limit for a given $H_k\cdots H_l$ interaction. For conformational analysis of glycosidic linkages, it is convenient to use a Ramachandran-type representation,[29] where distance constraints for each atom pair (derived from NOE data in our scheme) are mapped in the form of $\Phi,\Psi$ coordinates. This procedure is straightforward only for those atom pairs whose separation depends solely on these two torsional angles. When the contact refers to proton(s) of pendent groups (hydroxyl, hydroxymethyl, amido), the separation depends not only on $\Phi$ and $\Psi$ but also on up to four additional degrees of freedom, as in the case of hydroxyl protons of two hydroxymethyl groups. In order to rationalize the averaging pertinent to pendent groups alone, consider for the moment the glycosidic linkages as rigid. A reasonable model is to assume a very fast jumping, on the picosecond time scale, of pendent proton(s) $H_k(H_l)$ among possible equilibrium positions.[3f] The effective distance, averaged over pendent group rotation(s), can be expressed as[30]

$$r_{kl}(\text{eff}) = [(4\pi/5)\sum_{n=-2}^{2} |\sum_i \langle p_i \rangle Y_{2n}(\Phi_i) r_i^{-3}|^2]^{-1/6} \quad (4)$$

where $\langle p_i \rangle$ are the equilibrium populations of pendent proton(s), $r_i$ is the $H_k\cdots H_l$ interproton distance in conformation i, and $Y_{2n}(\Phi_i)$ are the spherical harmonic functions describing the orientation of $r_i$ relative to some fixed frame in the molecule. Equation 4 can be used directly for mapping $r^*_{kl}$ into the $\Phi,\Psi$ coordinates. The angular terms in eq 4 can be dropped because their inclusion would only have lessened its numerator, the consequence being that the upper $r^*_{kl}$ limit would have obtained an additional safety margin and remained valid (cf. discussion of Figure 1). The calculation of the lower effective distance limit was based on the

(17) Williamson, M. P.; Neuhaus, D. *J. Magn. Reson.* **1987**, *72*, 369–375.
(18) Davis, D. G. *J. Am. Chem. Soc.* **1987**, *109*, 3471–3472.
(19) Fejzo, J.; Zolnai, Z.; Macura, S.; Markley, J. L. *J. Magn. Reson.* **1989**, *82*, 518–528.
(20) Farmer, B. T., II; Macura, S.; Brown, L. R. *J. Magn. Reson.* **1988**, *80*, 1–22.
(21) Bax, A. *J. Magn. Reson.* **1988**, *77*, 134–147.
(22) Griesinger, C.; Ernst, R. R. *J. Magn. Reson.* **1987**, *75*, 261–271.
(23) Macura, S.; Farmer, B. T., II; Brown, L. R. *J. Magn. Reson.* **1986**, *70*, 493–499.
(24) (a) Bax, A.; Sklenar, V.; Summers, M. F. *J. Magn. Reson.* **1986**, *70*, 327–331. (b) Farmer, B. T., II; Macura, S.; Brown, L. R. *J. Magn. Reson.* **1987**, *72*, 347–352.
(25) Borgias, B. A.; James, T. L. *J. Magn. Reson.* **1988**, *79*, 493–512.
(26) Poppe, L.; Dabrowski, J.; von der Lieth, C.-W.; Kolke, K.; Ogawa, T. *Eur. J. Biochem.* **1990**, *189*, 313–325.
(27) Jardetzky, O. *Biochim. Biophys. Acta* **1980**, *621*, 227–232.
(28) Braun, W. *Q. Rev. Biophys.* **1987**, *19*, 115–157.
(29) Cantor, C. R.; Schimmel, P. R. *Biophysical Chemistry*; W. H. Freeman and Co.: San Francisco, 1980; pp 253–260.
(30) Tropp, J. *J. Chem. Phys.* **1980**, *72*, 6035–6046.

sum of vdW radii in each of the pertinent combinations involving one or two heavy atoms of the pendent groups (HO···HC, HO···OH, HO···C-$H_2OH$, and $HOH_2C$···$CH_2OH$).

The distance mapping procedure, which is a part of the SUGAR program,[31] is schematically depicted in Figure 1. The $\Phi,\Psi$ coordinates are represented by a grid in intervals of 10°. For each grid point a distance between two protons, kl, was calculated; when their separation depended on glycosidic bond torsions only, this was a direct $r_{kl}$ distance, but if the separation was also a function of pendent group(s) torsions, $r_{kl}$(eff) was calculated with eq 4. The distance map for each kl contact was obtained as a projection, on the $\Phi,\Psi$ plane, of cross-sections of the distance surface cut at $r^*_{kl}$ and $r_{kl}$(min) defined above.

If, alternatively, a microsecond time scale for internal motions were to be assumed, the calculation of the $\langle r^{-6}\rangle^{-1/6}$ average, instead of the $\langle r^{-3}\rangle^{-1/3}$ one, would move down the distance surface, hence the cross-section at $r^*_{kl}$ would be larger. The difference is small, however, with insignificant effect on the final conclusions. On the other hand, angular terms in eq 4 would move the whole surface upwards, hence, contrarily, the cross sections would shrink: thus, the larger ones, calculated by neglecting these terms, would remain valid as a safer upper boundary.

The above distance mapping approach is based on the assumption that conformational changes of glycosidic linkages are slower than molecular tumbling.[32a,b] If this were not true, the net effect of radial and angular averaging (eq 4) would be to flatten the surface, so that a larger set of $\{\Phi,\Psi\}$ values would satisfy the measured NOE distance $r^*_{kl}$, and some of the otherwise separate $\{\Phi,\Psi\}$ regions would overlap. In consequence it would be even more difficult to decide whether the model of fast switching between two $\{\Phi,\Psi\}$ subsets or that of large-amplitude torsions around some average $\{\Phi,\Psi\}$ subset is correct. This ambiguity can probably be resolved by advanced energy minimum calculations.

The common areas for $\{\Phi,\Psi\}$ sets obtained for each atom pair were considered as defining the most probable conformations of the relevant part of the molecule. Although by neglecting $r_{kl} > r^*_{kl}$ we abandon attempts to find all possible conformations, we gain in reward some confidence that the conformation(s) found in the regions just described are the real ones, provided these regions are energetically allowed.

An alternative to demarcating allowable regions by energy calculations is to define them on the basis of geometric criteria, as in the original Ramachandran maps referring to dipeptides.[29] For the disaccharide segments of globoside, we checked all interatomic distances during rotation, in 10° steps, of the $\Phi$ and $\Psi$ angles. Using Ramachandran values, however, we obtained sterically allowed areas that were much more restricted than those corresponding to "relaxed" energy maps calculated for cellobiose and maltose, which allowed for relief of steric stress with small variations of atomic positions.[3d,e] For this reason, we lowered the minimum possible interatomic separations down to the point where sterically allowed areas resembled the "relaxed" energy maps obtained for these two disaccharides. In this way, possible deviations from the ideal $^4C_1$ geometry were roughly taken into account. In Figure 3a–e these areas are hatched. The interatomic separations (Å) used for all disaccharide fragments of globoside were as follows: C–C = 2.7; C–O = 2.4; C–N = 2.5; C–H = 1.9; O–O = 2.4; O–N = 2.3; O–H = 1.9; N–N = 2.3; H–H = 1.6. These distances are smaller by 0.3 Å than the minimum separations found in crystals of peptides.[29] The hydroxyl protons were not taken into account, and during the distance checking procedure all hydroxymethyl groups were kept in the *gt* conformation, while the acetamido group was held in the (−140°) conformation. The coordinates were taken from the Cambridge Crystallographic Data Bank, and computations were performed on an IBM 3090 computer.

The MM2(85) calculations were performed on the same computer. The minimization was carried out for over a hundred starting structures obtained from distance mapping, hard-sphere calculations, and randomly chosen $\Phi,\Psi$ angles. The starting conformations of pendent groups were chosen on the basis of experimental data referring to NOE and hydrogen bonding interactions and vicinal coupling constants (Tables II and III). Distance mapping was based on the NOE data presented in Table IV (cf. Figures 2, 4, 5, 7, and 8).

## Results and Discussion

**Conformation of Pendent Groups.** For exocyclic (hydroxymethyl) groups, three staggered positions are assumed to be allowed: *gg* (−60°), *gt* (60°), and *tg* (180°),[3a] with positive dihedral angles defined by the clockwise rotation of the C6–O6 bond, while viewing from the fixed O5–C5 bond along the C5–C6 rotation axis, in the O5–C5–C6–O6 bond sequence. For hydroxyl groups, the equilibrium positions are designated as *anti* (180°), $g^+$ (60°), and $g^-$ (−60°),[32b] dihedral angles being defined similarly by the H–O–C–H atoms in the case of secondary hydroxyl groups and H–O–C6–C5 in the case of primary ones. For the acetamido group, we assumed three minimum energy conformations with H–N–C–H dihedral angles equal to −140°, 120°, 60°.[3a] The rotamer populations of pendent groups can be derived from vicinal coupling constants with use of Karplus-type empirical equations, referring to hydroxymethyl,[33a,b] hydroxy,[34,35] and amido groups.[35,36]

**Table II.** Coupling Constants and Population Numbers for Exocyclic Groups in Globoside for $Me_2SO$, $Me_2NCHO$, and $D_2O$

| residue | solvent | $J_{H5H6R}$ | $J_{H5H6S}$ | populations | | |
|---|---|---|---|---|---|---|
| | | | | *gg* | *gt*[a] | *tg* |
| GalNAcβ-1V | $Me_2SO$ | 6.0 | 5.7 | 0.33 | 0.29 | 0.33 |
| | $Me_2NCHO$ | 6.2 | 5.9 | 0.30 | 0.30 | 0.40 |
| | $D_2O$ | 7.9 | 4.9 | 0.21 | 0.52 | 0.27 |
| Galα-1II | $Me_2SO$ | 6.1 | 6.0 | 0.29 | 0.29 | 0.42 |
| | $Me_2NCHO$ | 5.3 | 5.2 | 0.42 | 0.24 | 0.34 |
| | $D_2O$ | 6.7 | 6.7 | 0.20 | 0.32 | 0.48 |
| Galβ-1I | $Me_2SO$ | 6.8 | 7.0 | 0.19 | 0.31 | 0.50 |
| | $Me_2NCHO$ | 7.5 | 6.4 | 0.17 | 0.41 | 0.43 |
| | $D_2O$ | 7.9 | 4.5 | 0.23 | 0.54 | 0.23 |
| Glcβ-I | $Me_2SO$ | 4.8 | 2.3 | 0.63 | 0.32 | 0.05 |
| | $Me_2NCHO$ | 4.6 | 2.4 | 0.65 | 0.29 | 0.06 |
| | $D_2O$ | 3.7 | 2.0 | 0.74 | 0.22 | 0.04 |

[a] C6–O6 is gauche to C5–O5 and trans to C4–C5.

**Table III.** $^3J$ Coupling Constants (Hz), Temperature Coefficients, $\kappa$ ($-10^3$ ppm/deg C), and Populations for Hydroxy and Amido Protons of Globoside Dissolved in $Me_2SO$-$d_6$ and $Me_2NCHO$-$d_7$ (Italicized)

| residue | proton | $J$ | $\kappa$ | populations[a] | | |
|---|---|---|---|---|---|---|
| | | | | $p_1$ | $p_2$ | $p_3$ |
| GalNAcβ-1V | OH6 | 4.9; 6.0[b] | 5.0 | 0.33 | 0.33 | 0.33 |
| | | *5.9; 6.0* | *6.2* | *0.22* | *0.39* | *0.39* |
| | OH4 | 4.2 | 5.8 | 0.20 | 0.40 | 0.40 |
| | | *3.7* | *7.4* | *0.20* | *0.40* | *0.40* |
| | OH3 | 5.8 | 4.3 | 0.40 | 0.40 | 0.20 |
| | | *4.9* | *5.3* | *0.30* | *0.50* | *0.20* |
| | NH | 7.8 | 3.8 | 0.60 | 0.40 | 0.0 |
| | | *7.3* | *4.9* | *0.60* | *0.40* | *0.0* |
| Galα-1II | OH6 | 5.4; 5.4 | 4.3 | 0.33 | 0.33 | 0.33 |
| | | *5.4; 5.4* | *6.2* | *0.33* | *0.33* | *0.33* |
| | OH4 | 4.7 | 4.5 | 0.26 | 0.37 | 0.37 |
| | | *3.6* | *7.2* | *0.20* | *0.40* | *0.40* |
| | OH2 | 5.9 | 5.7 | 0.40 | 0.40 | 0.20 |
| | | *6.4* | *7.6* | *0.40* | *0.40* | *0.20* |
| Galβ-1I | OH6 | 5.4; 5.4 | 4.7 | 0.33 | 0.33 | 0.33 |
| | | *6.5; 6.0* | *5.9* | *0.16* | *0.40* | *0.44* |
| | OH3 | 5.9 | 7.1 | 0.40 | 0.40 | 0.20 |
| | | *6.4* | *6.5* | *0.50* | *0.30* | *0.20* |
| | OH2 | 4.9 | 6.4 | *0.30* | *0.50* | *0.20* |
| | | *3.7* | *7.8* | *0.20* | *0.40* | *0.40* |
| Glcβ-I | OH6 | 6.1; 6.1 | 5.8 | 0.20 | 0.40 | 0.40 |
| | | *6.7; 6.2* | *6.1* | *0.15* | *0.41* | *0.44* |
| | OH3 | 1.5 | 2.6 | 0.0 | 0.50 | 0.50 |
| | | *1.5* | *2.3* | *0.0* | *0.30* | *0.70* |
| | OH2 | 3.7 | 5.6 | 0.20 | 0.40 | 0.40 |
| | | *3.7* | *7.8* | *0.20* | *0.40* | *0.40* |

[a] For hydroxyl protons, $p_1$, $p_2$, and $p_3$ correspond to dihedral angles of 180°, 60°, and −60°, defined by H–O–C–H atoms for secondary hydroxy groups and by H–O–C–C for primary ones; for the NH proton, corresponding dihedral angles are −140°, 120°, and 160° defined by the H–N–C–H atoms. The largest standard deviation does not exceed 50% of the population value. [b] Two values correspond to $J_{OH,HR}$ and $J_{OH,HS}$.

(31) Lieth, C. W.; Schmitz, M.; Poppe, L.; Hauck, M.; Dabrowski, J. In *Software-Entwicklung in der Chemie 3*; Gauglitz, G., Ed.; Springer: Berlin, 1989; pp 371–378.

(32) (a) Kessler, H.; Griesinger, C.; Leutz, J.; Müller, A.; van Gunsteren, W. F.; Berendsen, H. J. C. *J. Am. Chem. Soc.* **1988**, *110*, 3393–3396. (b) Govil, G.; Hosur, R. V. In *NMR. Basic Principles and Progress*; Diehl, P., Fluck, E., Kosfeld, R., Eds.; Springer: Berlin, 1982; Vol. 20, pp 1–216.

(33) (a) Haasnoot, C. A. G.; de Leeuw, F. A. A. M.; Altona, C. *Tetrahedron* **1980**, *36*, 2783–2790. (b) Ohrui, Y.; Nishida, Y.; Watanabe, M.; Mori, M.; Meguro, H. *Tetrahedron Lett.* **1985**, *26*, 3251–3254.

(34) Fraser, R. R.; Kaufman, M.; Morand, P.; Govil, G. *Can. J. Chem.* **1968**, *47*, 403–409.

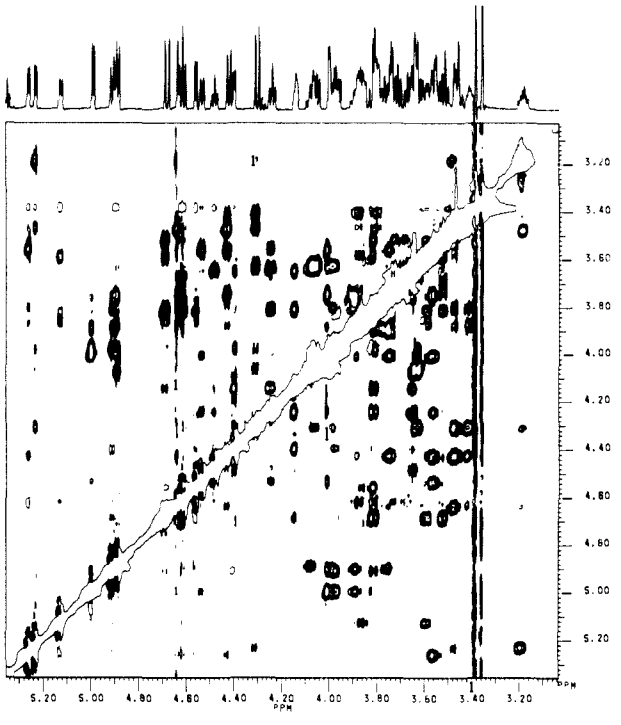

Figure 2. Expansion of the 2D ROESY spectrum of globoside in $Me_2NCHO$-$d_7$ solution at 310 K. Mixing time was 200 ms, offset for spin-locking was placed at 6.65 ppm, and lock-field strength was 2.5 kHz. The time domain spectra were multiplied with a cosine squared function.

With hydroxymethyl groups, assigning the prochiral methylene protons (*pro-R*, and -*S*) is a prerequisite. In the present study we adopted for the Glc and α- and β-Gal residues the assignments made for the same residues in globotriaosylceramide, and for the β-GalNAc residue we used the same assignments as for the β-Gal residue.[26] Vicinal coupling constants, measured from 1D HOHAHA and 1D COSY spectra, and calculated populations for exocyclic groups are shown in Table II. Coupling constants for hydroxyl protons and temperature shift coefficients for these protons are in Table III. The populations for primary hydroxy groups were calculated on the basis of vicinal coupling to both prochiral protons. For secondary hydroxy groups that showed interresidual NOE contacts, populations were estimated by means of multilinear regression analysis, using vicinal coupling constants and effective distances to the neighboring ring protons as experimental variables. The multiple correlation coefficients of the fits were in the 0.9–0.98 range. The values found in this way are thus consistent with the NOE data and with the chosen definition of pendent group conformation (vide supra).

**Conformation of the GalNAcβ1-3Galα (IV → III) Segment.** The Φ,Ψ map of NOE contacts for this linkage is shown in Figure 3a. The areas marked by large filled circles highlight the regions of conformational space where several NOE-derived constraints overlap with one another and with geometrically allowed regions, thus indicating the most probable conformers. The acetamido group was estimated to occupy the −140° and +120° conformations in a 60:40 ratio, and the optimized minimum energy geometries indicated the possibility of hydrogen bond formation between the carbonyl oxygen and IVOH3, IIIOH2, and IIIOH4 protons. The last two of these hydrogen bonds appear to be confirmed by the large (ca. 0.28 ppm) upfield shift observed in $Me_2SO$ for IIIOH2 and IIIOH4 when going from globotriaosylceramide,[26] where Gal-III is terminal and these hydroxy groups are solvated by the strong proton-acceptor $Me_2SO$, to globoside, where they can be engaged in hydrogen bonding with the amido carbonyl of the new terminal residue, GalNAc. Accordingly, no analogical chemical shift differences were observed

Table IV. Interresidual NOE Contacts for Globoside[a] Obtained from 2D ROESY Spectra for $Me_2SO$-$d_6$ and $Me_2NCHO$-$d_7$ Solutions and 2D NOESY and ROESY Spectra for the $D_2O$/DPC Solution

| | r*, Å | | |
|---|---|---|---|
| proton pair | $Me_2SO$ | $Me_2NCHO$ | $D_2O$/DPC |
| IVH1/IIIH3 | 2.3 | 2.3 | 2.3 |
| IVH1/IIIH4 | 3.1 | 3.1 | 3.3 |
| IVH1/IIIH2 | 3.7 | 3.7 | 3.5 |
| IVH1/IIIOH2 | 3.3 | 3.3 | |
| IVOH6/IIIH4 | 4.3 | 4.3 | |
| NH/IIIOH2 | 3.2 | 3.1[b] | |
| IIIH1/IIH4 | 2.4 | 2.3 | 2.4 |
| IIIH1/IIH6R | 2.7 | 2.7 | 2.6 |
| IIIH1/IIOH3 | 3.5 | 3.2 | |
| IIIH5/IIH2 | 2.9 | 2.7 | 2.5 |
| IIIH5/IIH4 | 3.6 | 3.6 | 3.7 |
| IIIH5/IIOH3 | 2.7 | 2.9 | |
| IIIOH2/IIH6S | 3.2 | 3.2 | |
| IIIOH2/IIOH6 | 3.5[c] | n.d.[d] | |
| IIIOH6/IIOH3 | 3.3 | n.d.[c] | |
| IIH1/IH4(3,5) | 2.2 | 2.2 | 2.2 |
| IIH1/IH6S | 3.7 | 3.4 | 3.6 |
| IIH1/IOH6 | 3.9 | 4.0 | |
| IIH1/IOH3 | 3.4 | 3.1 | |
| IIH5/IOH3 | 3.2 | 3.1 | |
| IIH6S/IOH3 | 3.5 | 3.5 | |
| IIOH6/IOH3 | 3.4 | 3.6 | |
| IIOH2/IOH6 | 3.1 | 3.2 | |
| IIOH2/IH6R | 3.5 | 3.5 | |
| IIOH2/IH6S | 3.5 | 3.5 | |
| IIOH2/IOH3 | 3.5 | 3.5 | |

[a] For labeling see Tables I–III. [b] Doubling of the NH signal for a partly deuterium exchanged sample due to the deuterium isotope effect. [c] Deuterium isotope effect. [d] Not determined.

in $Me_2NCHO$ solutions,[37] as the effects of hydrogen bonding with acetamido and formamido carbonyl groups must be very similar. At the same time, hydrogen bonding between the amido proton and the IIIO2 oxygen was evidenced by doubling[38] of the NH signal to $Me_2NCHO$, due to the isotope effect, and broadening in $Me_2SO$ solutions, observed for a ca. 50% deuterated sample. The expected reciprocal isotope effect on the IIIOH2 proton was not observed, probably due to its competing interaction with IIOH6 (cf. III → II conformation).

The experimental and computational data suggest that a number of hydrogen bonds exist in the following conformers obtained by torsions about the Φ, Ψ, and H–N–C–H angles (listed in this order): IVOH3···OC and NH···IIIO2 in the (20°, 40°, −140°) conformation; IIIOH4···OC in the (20°, 40°, 120°) conformation; IIIOH2···OC in the (30°, −50°, 120°) conformation. These results show the glycosidic angle Ψ to vary over a span of 90°, whereas the Φ angle remains almost unchanged.

Apart from the torsions of the *N*-acetamido group around the N–C bond to the ring, we observed a small amount of the amide *E* isomer in both $Me_2SO$ and $Me_2NCHO$ solutions. This minor component was identified by ROESY exchange cross peaks between some of its resonances and the corresponding resonances of the dominant *Z* isomer; clearly visible were the NH, IVH2, IVH1 (only in $Me_2NCHO$), IVOH3, and IIOH2 cross peaks. The exchange was slow and at 290 K practically unnoticeable in both solvents. The *Z*:*E* ratio was about 40:1.

**Conformation of the Galα1-4Galβ (III → II) Segment.** The NOE map for this linkage (Figure 3b,c) shows that possible conformations are characterized by glycosidic bond angles around (−40°,−10°) and (−10°,40°). Practically the same values were obtained in a similar study of globotriaosylceramide, and the populations of these conformers were found to be approximately the same in $Me_2SO$ and $D_2O$ solutions.[26] In the case of globoside, however, the population ratio of these two conformers in $Me_2SO$

(35) Scott, J. E.; Heatley, F.; Hull, W. E. *Biochem. J.* **1984**, *220*, 197–205.
(36) Bystrov, V. F.; Portnova, S. L.; Balashova, T. A.; Kozmin, S. A.; Gavrilov, Y. D.; Afanasev, V. A. *Tetrahedron* **1973**, *29*, 873–877.
(37) The data on $Me_2NCHO$ solutions of globotriaosylceramide have not been published.
(38) Lemieux, R. U.; Bock, K. *Jpn. J. Antibiot. Suppl.* **1979**, *32*, 163–177.

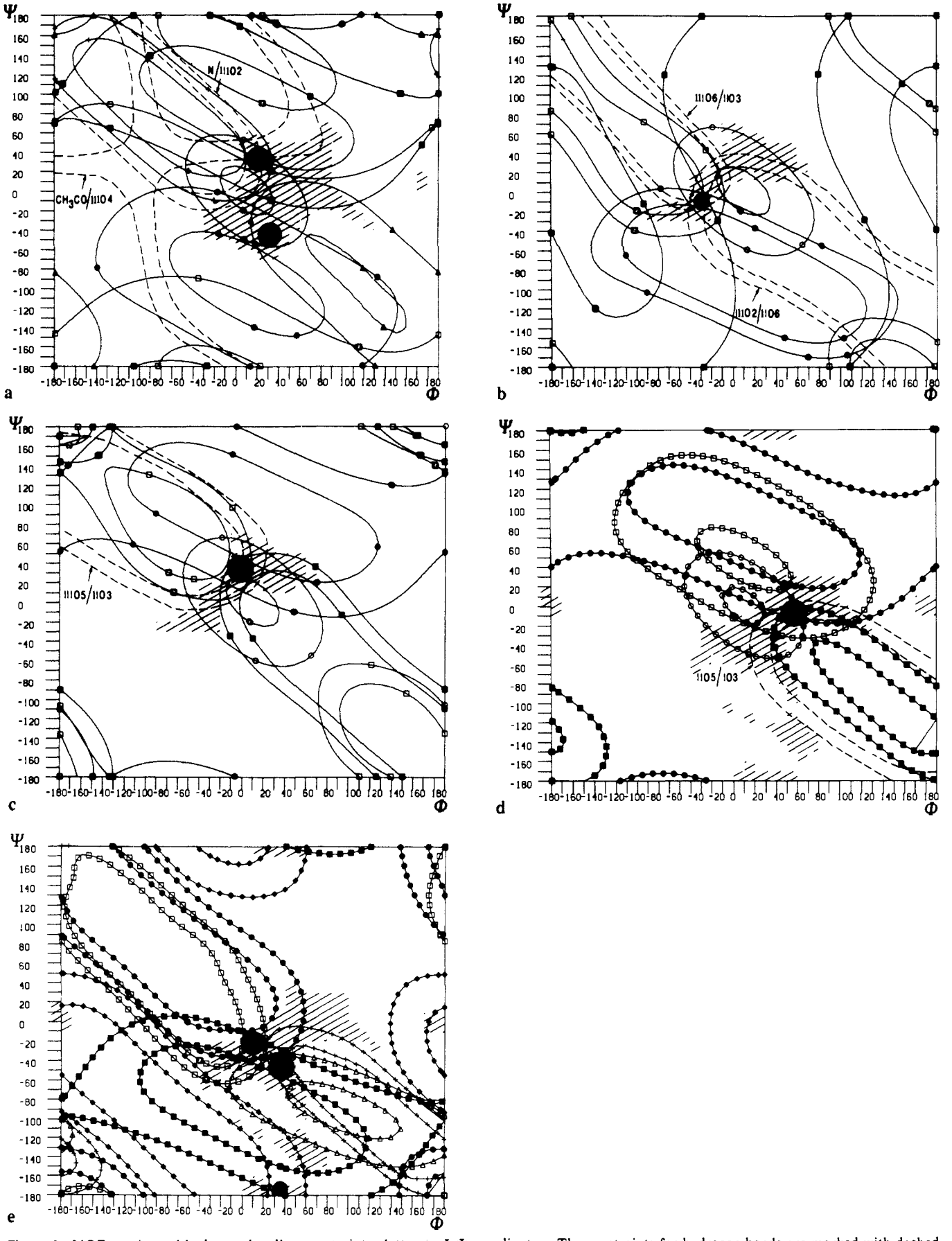


Figure 3. NOE, steric, and hydrogen-bonding constraints plotted in Φ,Ψ coordinates. The constraints for hydrogen bonds are marked with dashed lines, and sterically allowed areas are hatched. (a) GalNAcβ1-3Galα linkage. NOE contacts are marked with the following symbols: (■) 1VH1/1IIOH2; (□) 1VH1/1IIH2; (+) NH/1IIOH2; (△) 1VOH6/1IIH4; (●) 1VH1/1IIH4; (○) 1VH1/1IIH3. (b) Galα1-4Galβ linkage: (○) 1IIH1/1IH4; (●) 1IIH1/1IH6*R*; (□) 1IIH5/1IOH3; (■) 1IIH5/1IH4. (c) Galα-4Galβ linkage: (○) 1IIH1/1IH4; (●) 1IIH1/1IOH3; (□) 1IIH5/1IH2; (■) 1IIOH2/1IH6*S*. (d) Galβ1-4Glcβ linkage: (○) 1IH1/1H4; (●) 1IH1/1H6*s*; (□) 1IH1/1OH6; (■) 1IH6*s*/1OH3. (e) Galβ1-4Glcβ linkage: (●) 1IOH2/1H6*s*; (□) 1IOH2/1OH6; (△) 1IH5/1OH3; (■) 1IH1/1OH3; (+) 1IOH6/1OH3; (⊠) 1IOH2/1OH3.

differs from that found in $Me_2NCHO$ and $D_2O$ solutions, thus suggesting that the conformation of this disaccharide segment is affected both by the solvent and, indirectly, by the peripheral GalNAc-IV residue. These conclusions were drawn from the different behavior of several resonances of these two compounds in different solvents, which can be summarized as follows:

(a) The IIIH1/IIOH3 and IIIH5/IIH2 dipolar interactions characteristic of the (−10°,40°) conformer are weaker in $Me_2SO$ than in $Me_2NCHO$ and also weaker than those observed for triaosylceramide dissolved in either $Me_2SO$, $Me_2NCHO$,[37] or $D_2O$.

(b) Deshielding of the IIIH5 proton by the IIO3 oxygen, which is only ~2.3 Å apart in the (−40°,−10°) conformer and ~3.0 Å in the (−10°,40°) one, can also be used as a criterion for changes of the equilibrium between these conformers. The fact that IIIH5 is deshielded in globoside vs triaosylceramide by 0.12 ppm in $Me_2SO$, and only by 0.06 ppm in $Me_2NCHO$ or $D_2O$, is clearly indicative of equilibrium shifts.

(c) In our previous study we postulated the hydrogen bond formation between the IIOH3 proton and the ring oxygen, IIIO5, of the αGal residue. This hydrogen bond was found in crystalline galabiose[39] and can preferentially be formed in the (−10°,40°) conformer (Figure 3c). For globoside vs triaosylceramide, both dissolved in $Me_2SO$, the IIOH3 resonance is shifted about 0.2 ppm to lower field, shows twice as large a temperature coefficient, and shows a coupling constant that is smaller by ~2 Hz. All these observations point to a weaker IIOH3/IIIO5 interaction and stronger solvation of this proton by $Me_2SO$ in globoside, as compared with triaosylceramide. In $Me_2NCHO$ solution, these differences are insignificant.

(d) The IIIOH2···IIOH6 hydrogen bonding found in the previous study[26] is also present in globoside dissolved in $Me_2SO$; the isotope effect occurs only for proton IIOH6, however, and is smaller from that observed for triaosylceramide (1.4 vs 2.5 Hz; cf. IV → III conformation). In $Me_2NCHO$, the IIIOH2 signal was also not split and the IIOH6 one was overlapped at all temperatures. At the same time, both of the IIIOH6 and IIOH3 protons showed small isotope effects (~1.2 Hz), demonstrating the hydrogen bonding, not observed in $Me_2SO$, which can form in the (−40°,−10°) conformer (see Figure 3b).

**Conformation of the Galβ1-4Glcβ (II → I) Segment.** This linkage occurs in almost all series of glycosphingolipids and is closely related to that occurring in cellobiose, Glcβ1-4Glcβ, a disaccharide subjected recently to a number of experimental and theoretical investigations, summarized in ref 40.

As with other disaccharide segments, the number of NOE contacts is much larger when hydroxyl groups are included in the analysis (see Table I). For the purpose of clarity, the constraints defining one of the conformations were plotted separately in Figure 3d–e. The most probable sets of {Φ,Ψ} angles sampled by this linkage are in the vicinity of (55°,0°), (35°,−50°), and (5°,−30°) values. As found with triaosylceramide,[26] the IOH3···IIO5 hydrogen bond is indicated by a vanishingly small coupling constant, the lowest temperature shift coefficient, and the lowest deuterium exchange rate for the IOH3 proton. All these features are common to both the $Me_2NCHO$ and $Me_2SO$ solutions; however, in the latter solvent this hydrogen bond might be less populated, because the $g^-$ conformation of the hydroxyl group is less populated (see Table III). The constraint for IIO5···IOH3 is plotted in Figure 3d, and it seems very probable that this hydrogen bond survives transitions between the (55°,0°) and (35°,−50°) conformations but breaks in the (5°,−30°) conformation (cf. parts d and e of Figure 3). The latter is proved by a relatively strong NOE interaction between the relevant protons (IIOH2/IOH6) in $Me_2SO$ solution, shown in Figure 4. In the same figure we show the IIOH6/IOH3 NOE interaction, which may arise from cooperative hydrogen bonding, involving the IIOH6···IO3 and IOH3···IIO5 bonds.

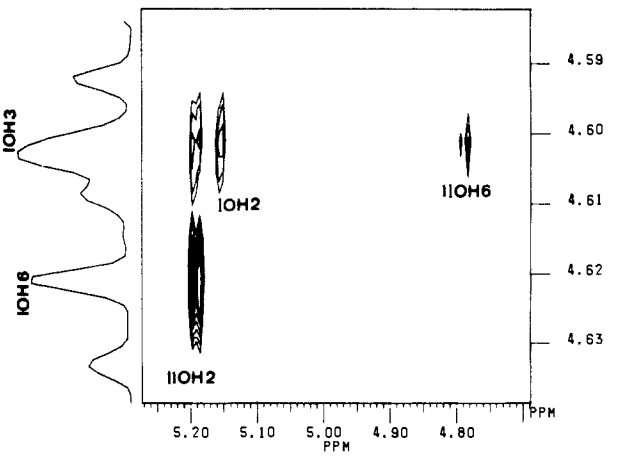


Figure 4. Expansion of a selective, $\omega_1$-decoupled 2D ROESY spectrum of globoside in $Me_2SO$-$d_6$ solution at 291 K.

The most interesting observation is the NOE contact between the IIOH2 and IOH3 protons (Figure 4), since this implies that either the angle Φ or Ψ is close to 180° (see Figure 3d), i.e., it refers to conformations that have been much disputed in the literature. Thus, molecular mechanics calculations reported for cellobiose by several groups[3c,e] have predicted additional low-energy minima in the vicinity of (170°,0°) and (30°,180°) values, and in a NOE study of α-cellobiose 1-phosphate in $D_2O$ solution, combined with hard-sphere calculations, the occurrence of 10% of the (30°,180°) conformation was communicated.[41] In contrast, Praly and Lemieux[42] recapitulated the arguments in favor of the existence of substantially rigid oligosaccharide structures. Since the IIOH2/IOH3 contact can be considered as direct proof of one or both of the "trans" (180°) conformations, we took pains to demonstrate their presence with utmost certainty. Therefore, the ROESY spectrum was measured with a high digital resolution and $\omega_1$ decoupling, in order to separate the partly overlapping IIOH2/IOH3, IIOH2/IOH6, and IOH2/IOH3 cross-peaks (Figure 4). Independently, this diagnostic IIOH2/IOH3 NOE was observed in a 1D ROE spectrum of the $Me_2NCHO$ solution recorded at 263 K, where the selectively irradiated IIOH2 resonance was well separated, and exchange phenomena were practically eliminated. Unfortunately, it was not possible to corroborate these results by NOEs referring to unexchangeable, C-linked protons; as in all solvents used in our experiments the H3, H4, and H5 resonances of the Glc-I unit were overlapped closely, and hence it could not be decided whether IIH1 interacted exclusively with IH4 or rather also with IH5 and IH3, as required for the (30°,180°) conformation. This summated IIH1/I(H3+H4+H5) NOE is excessively strong, however, with respect to the IIH1/IH4 interaction alone, implying an unacceptably short distance between these atoms, hence it can be assumed to contain a contribution from the IIH1/I((H3+H5) interactions as well.

The pronounced flexibility of this linkage demonstrated in this work has also been revealed by optical rotation studies[40] and theoretical calculations.[3c-e]

**Conformation of the Entire Oligosaccharide Chain.** For modeling its 3D structure we used the molecular mechanics MM2(85) program, with input conformations of the disacharide fragments defined on the basis of NOE constraints and marked by large filled circles in Figure 3a–e. The conformations of pendent groups, specified in footnotes in Table V, were chosen as described in Methods. Since the aim of our calculations was to test the reliability of the structures derived by using the distance mapping procedure, we refrained from the prohibitively time-consuming detailed exploration of conformational space of the whole molecule; instead, several additional calculation trains were started from randomly chosen geometries and from those obtained in earlier

(39) Svensson, G.; Albertsson, J.; Svensson, C.; Magnusson, G.; Dahmen, J. *Carbohydr. Res.* **1986**, *146*, 29–38.
(40) Stevens, E. S.; Sathyanarayana, B. K. *J. Am. Chem. Soc.* **1989**, *111*, 4249–4254.
(41) Lipkind, G. M.; Shashkov, A. S.; Kochetkov, N. K. *Carbohydr. Res.* **1985**, *141*, 191–197.
(42) Praly, J. P.; Lemieux, R. U. *Can. J. Chem.* **1987**, *65*, 213–223.

**Table V.** Minimum Energy Conformations[a] (<−5 kcal/mol) Obtained for the Oligosaccharide Part of Globoside Obtained from MM2(85)[b] Calculations

| GalNAcβ1 → | 3Galα1 | → | 4Galβ1 | → | 4Glcβ | |
|---|---|---|---|---|---|---|
| Φ | Ψ | Φ | Ψ | Φ | Ψ | E |
| 34.1 | −53.5 | −12.9 | 40.4 | −8.0 | 28.3 | −10.9 |
| 24.8[d] | 41.2 | −14.8 | 42.6 | 175.0 | −5.66 | −10.8 |
| 35.3 | −57.3 | −36.9 | −16.4 | 66.2 | −6.8 | −9.7 |
| 32.7 | −57.6 | −37.8 | −12.2 | 50.5 | 4.7 | −9.4 |
| 32.0 | −57.9 | −41.2 | −11.2 | 165.4 | 2.3 | −9.3 |
| 27.8[c] | 33.0 | −39.1 | −13.2 | 172.0 | 2.3 | −9.2 |
| 35.4 | −55.8 | −17.4 | 33.8 | 40.8 | −18.8 | −9.1 |
| 28.7[d] | 48.7 | −31.1 | −24.0 | 58.6 | −0.2 | −8.4 |
| 15.8 | −53.6 | −12.4 | 37.0 | −4.5 | −32.0 | −8.2 |
| 34.2 | −55.0 | −13.2 | 41.4 | 52.9 | 5.3 | −8.0 |
| 30.2 | −54.0 | −12.6 | 33.3 | 19.2 | −20.0 | −7.9 |
| 11.2 | −54.3 | −11.0 | 38.5 | 2.3 | −28.4 | −7.9 |
| 33.5 | −55.7 | −13.9 | 38.5 | 29.5 | −41.2 | −7.8 |
| 24.1[d] | 45.2 | −18.2 | 39.8 | 54.4 | 2.55 | −7.8 |
| 24.7[d] | 48.2 | −15.3 | 40.3 | 55.5 | 2.5 | −7.6 |
| 29.3 | −57.4 | −38.1 | −12.5 | −5.5 | −34.9 | −7.5 |
| 32.4 | −56.7 | 1.0 | 38.6 | 69.5 | −4.5 | −7.3 |
| 31.2 | −59.3 | −38.1 | −12.5 | 36.7 | −41.8 | −7.1 |
| 32.6 | −55.9 | −4.3 | 41.5 | 9.5 | −29.0 | −6.0 |
| 22.4[c] | 33.4 | −17.2 | 40.3 | 70.1 | −3.3 | −5.3 |

[a] The hydroxymethyl groups were held in the *gt* conformation for Galα and in *gg* for all other residues. Unless otherwise remarked, the amido group was input in the 120° conformation (after energy minimization, ∠H-N-C-H was equal to 135°) and the IIIOH2 group in the $g^+$ conformation. [b] Dielectric constant $\epsilon = 1.5$. [c] The amido group in the −140° conformation (−137° obtained after minimization) and the IIIOH2 group in the anti conformation. [d] The IIIOH2 group in the anti conformation.

molecular mechanics[7b] and hard-sphere[7a,43a] minimum-energy calculations for globoside. All but one lowest energy conformations listed in Table V overlap with experimentally derived structures. In one case, the energy minimization converged to a low-energy structure (−13.9 kcal/mol), characterized by Φ,Ψ glycosidic angles (IV–III: 177.7, 49.5; III–II: −27.5, 4.1; II–I: 5.1, 4.5), which fall outside the NOE-derived regions in the Φ,Ψ space of each linkage (cf. Figure 3a–e), rendering this conformation to be of little importance, if not a computational artefact. Furthermore, although the energy values listed in Table V were not optimized, and not too much significance should be attached to the concrete magnitude of their differences, it is remarkable that the minimum energy structures for the Galβ1-4Glc linkage in the (170°,−5°) conformation have exceptionally low energies, in contradiction to the low population of this and/or the other "trans" conformations found experimentally (cf. previous section). The reason for discrepancies of this type can be looked for in the circumstance that these minimum energy structures can result from allowing for bond angle deformations, which might compensate the otherwise unacceptably strong nonbonded interactions. Such is especially likely with longer oligosaccharide chains, whose sugar residues that are distant within the primary structure may come close together in space to produce a large number of nonbonded interactions. It also should be borne in mind that our MM2 energy calculations refer to vacuum, hence the problem of the possibly overemphasized contribution of these structures might not have arisen if spacing of sugar moieties by solvent molecules had been taken into account.

Convincing proof of the calculated overall structures is the long-range NOE contacts between methyl protons of the βGalNAc residue and the IIIOH2, IIOH6, and IOH3 protons in $Me_2SO$ solution (Figure 5). In $Me_2NCHO$, only the first two of these interactions were found with confidence. The stereodiagram of the conformer with energy −9.7 kcal/mol in Table V exhibiting

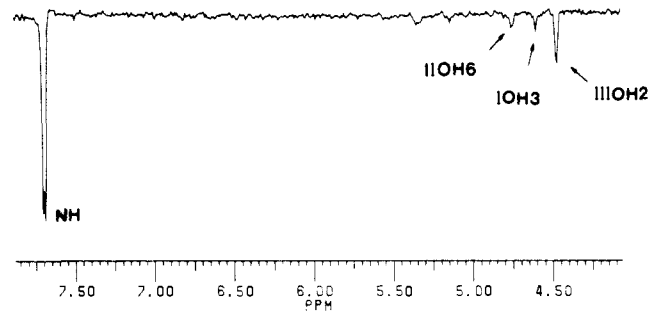


**Figure 5.** Cross-section through the methyl resonance in the 2D ROESY spectrum of globoside in $Me_2SO$-$d_6$ solution at 298 K.

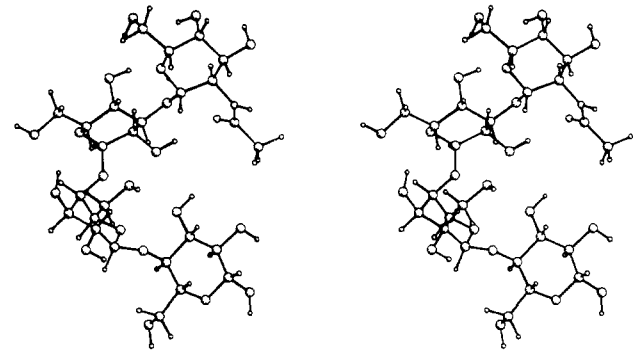

**Figure 6.** Stereodiagram of the low-energy conformer (−9.7 kcal/mol; Table V) obtained from MM2(85) calculations.

the IVNCOCH3/IOH3 interaction is shown in Figure 6.

The multiple conformations found in this study contrast with the structure predicted for globoside by HSEA calculations reported by Bock et al.[43a] Thus, only one conformation was obtained for each of the glycosidic bonds with use of this computational scheme, and this result was considered[43a] to be supported by experimental data, which were interpreted[43b] as referring to single conformations. Similar rigidity was postulated for the Galβ1-4Glc[44] and Galβ1-3GalNAc[44] linkages. On the other hand, branched, vicinally diglycosylated trisaccharide fragments of the oligosaccharide chain can be fixed in one conformation, due to through-space interactions between the two glycosidic substituents. Such was reported by Sabesan et al.[44] for the GalNAcβ1-(NeuAcα2-3)4Gal fragment of the GM1 ganglioside and corroborated by a large number of NOE contacts in our forthcoming paper.[45]

In contrast, Scarsdale et al. observed a few NOEs in addition to those referring to the two protons located directly at the glycosidic bridge and used them in the form of additional (pseudoenergy) terms in HSEA[7a] and MM2[7b] calculations. On the basis of these results, flexibility was inferred for the GalNAcβ1-3Gal[7a] and Galα1-4Gal[7b] linkages. However, all but one (Table V, item 3) minimum energy structure thus obtained differed from those reported in the present work, i.e. they would fall outside of the areas determined by our $r^*_{kl}$ NOE distances.

**Conformation of Micelle-Bound Globoside.** The glycolipid–phosphatidylcholine mixed micelles were prepared following the work of Eaton and Hakomori.[46] The detailed physicochemical studies of DPC micelles by Bösch et al.[47a,b] suggest that micellar aggregates are small and should contain about 40 molecules of detergent per 1 molecule of globoside. The motion of globoside, anchored in such micelle, is fast enough to produce narrow lines

(43) (a) Bock, K.; Breimer, M. E.; Brignole, A.; Hansson, G. C.; Karlsson, G. L.; Leffler, H.; Samuelsson, B. E.; Strömberg, N.; Svanborg-Edén, C.; Thurin, J. *J. Biol. Chem.* **1985**, *260*, 8545–8551. (b) Yu, R. K.; Koerner, T. A. W.; Demou, P. C.; Scarsdale, J. N.; Prestegard, J. H. *Adv. Exp. Med. Biol.* **1984**, *174*, 87–102.

(44) Sabesan, S.; Bock, K.; Lemieux, R. V. *Can. J. Chem.* **1984**, *62*, 1034–1044.

(45) Acquotti, D.; Poppe, L.; Dabrowski, J.; von der Lieth, C.-W.; Sonnino, S.; Tettamanti, G. Following paper in this issue.

(46) Eaton, H. L.; Hakomori, S. I. Third Chemical Congress of North America, Toronto, 1988; Abstract CARB 91.

(47) (a) Bösch, C.; Brown, L. R.; Wüthrich, K. *Biochim. Biophys. Acta* **1983**, *603*, 298–312. (b) Lauterwein, J.; Bösch, C.; Brown, L. R. *Biochim. Biophys. Acta* **1979**, *556*, 244–264.

**Table VI.** Nonselective ($R^{ns}$) and Selective ($R^{s}$) Relaxation Rates ($s^{-1}$) for Anomeric Protons of Globoside in DPC Micelles at 303 K (at 500 and 360 MHz) and the Calculated Motional Parameters[a] ($\tau_i$ (ns) and $S$ (see text))

| proton | $R^{ns}$(500) | $R^{ns}$(360) | $R^{s}$(500) | $R^{s}$(360) | $\tau_i$ | $S$ |
|---|---|---|---|---|---|---|
| IVH1 | 0.89 ± 0.03[b] | 1.42 ± 0.03 | 2.35 ± 0.15 | 2.75 ± 0.10 | 0.43 | 0.50 |
| IIIH1 | 0.77 ± 0.03 | 1.24 ± 0.03 | 2.82 ± 0.15 | 3.16 ± 0.07 | 0.42 | 0.60 |
| IIH1 | 0.65 ± 0.04 | 1.02 ± 0.03 | 5.60 ± 0.26 | 5.54 ± 0.27 | 0.36 | 0.83 |
| IH1 | 0.58 ± 0.05 | 0.91 ± 0.03 | 5.68 ± 0.24 | 5.34 ± 0.35 | 0.35 | 0.86 |

[a] The estimated $\tau_s$ (slow motion) value is equal to 5.5 ns. [b] Standard deviations.

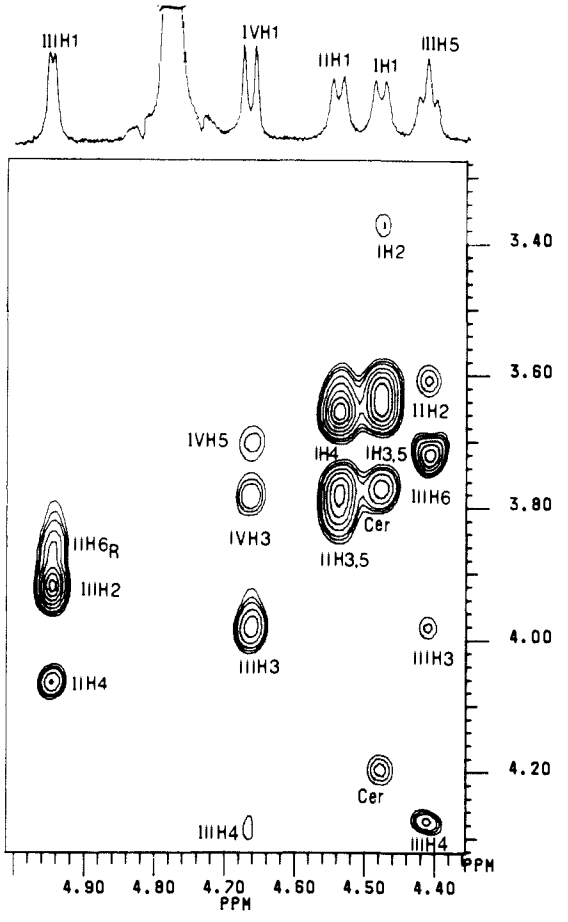


**Figure 7.** Expansion of the 2D NOESY spectrum of globoside in $D_2O$/DPC solution at 303 K. Mixing time was 100 ms and residual water signal was saturated with a long DANTE pulse during the relaxation delay. The time domain spectra were multiplied with a Lorentzian–Gaussian function. The IIIH1/IIH6s and IIIH5/IIH4 NOE contacts are below the lowest level plotted.

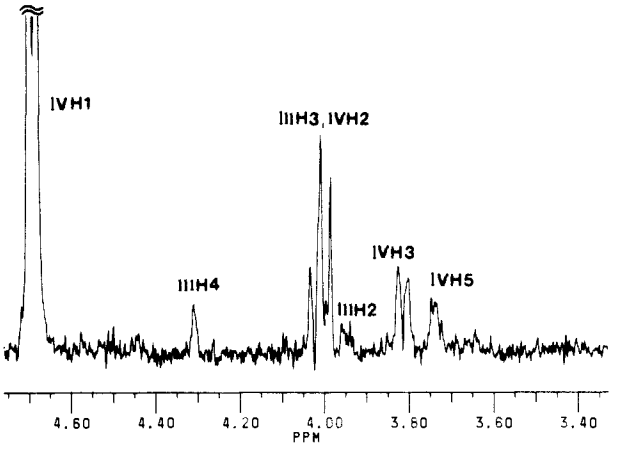


**Figure 8.** 1D NOESY experiment with selective inversion of the IVH1 proton using a 20-ms selective Gaussian pulse, mixing time of 50 ms, and read pulse of ~10°. The IIIH3 NOE response signal is overlapped by the IVH2 signal resulting predominantly from H1–H2 selective population transfer.[2] The number of transients was 3200, and the summated FID was multiplied with a Lorentzian–Gaussian function before transformation.

for sugar ring protons. The conformation of the glycosidic linkages was probed by 2D and 1D NOESY (Figures 7 and 8) and ROESY measurements, and interresidual distances calculated on the basis of eq 1 are in Table IV. The GalNAc$\beta$1-3Gal$\alpha$ linkage showed the same flexibility in aqueous solution as in $Me_2SO$ and $Me_2NCHO$ solutions. As before, the observed IVH1/IIIH4 and IVH1/IIIH2 NOE contacts (Figure 8) are characteristic of the (30°,−50°) and (20°,40°) conformers, respectively. The IVH1/IIIH2 correlation needs some comment, as it could also have arisen from scalar coupling effects,[48] operative on IIIH2 and IIIH3 protons ($J \approx 11$ Hz, $\Delta\nu \approx 37$ Hz), the latter being close in space to the IVH1 proton. This is, however, not the case, as the 1D transient NOE spectra were recorded with a small angle (ca. 10°) read pulse so that flip angle effects[48] are absent and the intensity of the IVH1/IIIH2 contact is still stronger by a factor 5 than would have resulted solely from the scalar coupling mechanism.

The number of NOE contacts for the Gal$\alpha$1-4Gal$\beta$ linkage (see Table IV and Figure 7) is sufficient to distinguish two different conformations, which are the same as in $Me_2SO$ and $Me_2NCHO$ solutions and for the oligosaccharide part of triaosylceramide in $D_2O$ solution.[26]

For Gal$\beta$1-4Glc$\beta$ linkage only two NOE contacts could be measured (Table IV). The IIH1/IH6 one, indicative of the (55°,0°) conformation, is weak, hence it could be speculated that other conformations must also be present, because otherwise this contact would be stronger. It must be admitted, however, that alternative interpretations are also possible, although, in view of the preserved flexibility of the IV–III and III–II linkages in water, there are no grounds to expect that the flexibility of this linkage differs substantially from that found in the two aprotic solvents.

**Globoside Mobility in Micelles.** Some insight into the dynamics of the carbohydrate chain of globoside can be gained by measuring relaxation rates of accessible protons at different magnetic fields. We chose for this purpose the anomeric protons of the four sugar units and measured their initial relaxation rates at 360 and 500 MHz after nonselective and selective inversion pulses.[49] The calculated rate constants are in Table VI. Since the cross-relaxation and cross-correlation effects[30,50] are negligible for short times after perturbation, the initial recovery of magnetization is governed by a single rate constant, which for nonselective and selective experiments can be expressed by eqs 5a and 5b, respectively:[49]

$$R^{ns} = K[3J(\omega) + 12J(2\omega)] \quad (5a)$$

$$R^{s} = K[J(0) + 3J(\omega) + 6J(2\omega)] \quad (5b)$$

where $K = 0.1\sum_l \gamma^4\hbar^2 r_{kl}^{-6}$, $\gamma$ being the gyromagnetic ratio for the proton, $\hbar$ the Planck constant, and $r_{kl}$ the distance between two protons relaxing by the dipolar mechanism. $J(n\omega)$, where $n$ = 0, 1, 2, are spectral densities, which depend on the type of molecular motion and Larmor frequency. For simplicity, we assumed the same motional dependence for all dipolar vectors originating from the anomeric proton k and analyzed the relaxation data in

(48) Keeler, J.; Neuhaus, D.; Williamson, M. P. *J. Magn. Reson.* **1987**, *73*, 45.

(49) Mirau, P. A.; Bovey, F. A. *J. Am. Chem. Soc.* **1986**, *108*, 5130–5134.

(50) Dais, P.; Perlin, A. S. *Adv. Carbohydr. Chem. Biochem.* **1987**, *45*, 125–168.

**Table VII.** Measured Cross-Relaxation Rates in the Laboratory and Rotating Frame for Chosen Proton Pairs in Globoside Dissolved in DPC/$D_2O$ at 303 K and the Values Calculated with Model-Free Parameters

| proton pair | $\sigma_{\parallel}$(exp) | $\sigma_{\parallel}$(calc) | $\sigma_{\perp}$(exp) | $\sigma_{\perp}$(calc) |
|---|---|---|---|---|
| IVH1/IVH5[a] | −0.25 | −0.33 | 0.75 | 0.87 |
| IVH1/IVH3[a] | −0.29 | −0.33 | 0.69 | 0.87 |
| IIIH5/IIIH4[b] | −0.55 | −0.60 | 1.25 | 1.42 |
| IIIH5/IIIH3[c] | −0.35 | −0.37 | 0.90 | 0.88 |
| IIH1/IIH5,H3[a] | −2.10 | −1.76 | 3.50 | 3.72 |
| IH1/IH5,IH3[a] | −2.35 | −1.89 | 3.60 | 3.96 |
| IH1/IH2[d] | −0.27 | −0.26 | 0.45 | 0.54 |

[a] $r$ = 2.5 Å. [b] $r$ = 2.4 Å. [c] $r$ = 2.6 Å. [d] $r$ = 3.1 Å.

terms of model-free motional parameters, where spectral densities are expressed through eq 6[51]

$$J(n\omega) = S^2\tau_s/(1 + n^2\omega^2\tau^2) + (1 - S^2)\tau_e/(1 + n^2\omega^2\tau^2) \quad (6)$$

where $\tau_s$ and $\tau_i$ are the correlation times for the slow overall motion and the internal motion, respectively, $\tau_e^{-1} = \tau_s^{-1} + \tau_i^{-1}$, and $S$ is the generalized order parameter. The internal and overall motions may be complex, but in this model they are grouped together into two correlation times, which approximate the effects of true motions. The order parameter is a measure of the spatial restriction of the internal motion. The set of $\tau_s$, $\tau_i$, $S$ parameters was chosen such (Table VI) as to give a minimum value for the following sum

$$\sum_{i,j}[\sigma_{\perp,\parallel}(\text{calc}) - \sigma_{\perp,\parallel}(\text{obs})]^2/\sigma_{ij}^2(\text{obs})$$

where $\sigma$(obs) are the measured cross-relaxation rates (Table VII) for proton pairs at the known distances and $\sigma$(calc) are the calculated cross-relaxation rates on the basis of eqs 7a and 7b.

$$\sigma_{\parallel} = K[6J(2\omega) - J(0)] \quad (7a)$$

$$\sigma_{\perp} = K[2J(0) + 3J(\omega)] \quad (7b)$$

The data in Table VI clearly show fast internal motion characterized by $\tau_i$ of the order of 0.4 ns, experienced by the sugar protons of globoside anchored in DPC micelles. At the same time, $S$ values show that the terminal GalNAc unit has significantly more motional freedom than the Glc-I unit directly bonded to the lipid chain. The slow motion of 5.5 ns includes the tumbling of the whole micelle and the lateral diffusion of the glycolipid molecule on the surface of the micelle.[52] The contribution from the latter type of motion can be safely ignored, as one can expect the diffusional coefficient for globoside, which is anchored by two lipophilic chains, to be even smaller than that measured for detergent molecules,[47] hence $\tau_s$ is dominated by the rotation of the micelles, which can be expressed by the Stokes–Einstein relationship[52]

$$\tau_s = 4\pi r^3\eta/kT \quad (8)$$

where $r$ is the radius of a spherical micelle, $\eta$ viscosity of solution, $k$ Boltzman constant, and $T$ temperature. The radius of the micelle, calculated on the basis of eq 8, is 19 Å, in good agreement with light-scattering studies of DPC micelles by Lauterwein et al.[47b]

Since undifferentiated motional dependence was assumed for the H–H vectors (vide supra), the data presented in Tables VI and VII are not suitable to test any specific models of internal motion. It is probable that the observed differences in relaxation rates are caused either by segmental motion of the oligosaccharide chain or fast axial rotation[53] of the L-shaped globoside (cf. Figure 6) anchored in the DPC micelle, although both processes may contribute to the observed 0.4-ns correlation time.

## Conclusions

The conventional NOE contacts between C-linked protons of the globoside were complemented by more numerous contacts involving its amido and hydroxy protons and used for mapping glycosidic angles vs interatomic distances. A significant flexibility was demonstrated in this way for all the glycosidic linkages in $Me_2SO$, $Me_2NCHO$, and $D_2O$ solutions. Different conformations are stabilized by different networks of intramolecular hydrogen bonds. The Gal1$\beta$-4Glc$\beta$ linkage appeared to have the largest torsional freedom, and this seems to be a common feature of all glycosphingolipids containing this disaccharide segment.[26,45]

In spite of its flexibility, the carbohydrate chain is held on the time average in a bent or "L" shape even in globoside anchored in DPC micelles—a model system resembling the biological membrane, where it experiences an axial rotation on a subnanosecond time scale.

The conformations reported in this paper showed that the HSEA model did not predict correctly the 3D structure of the sugar part of globoside, but more sophisticated molecular mechanics calculations, with continuing improvements in the force-field parametrization,[7b,54] are more promising for predicting reliable oligosaccharide conformations.

The analysis showed the ROESY experiment to be indispensable, in that it enables one to avoid misinterpretation due to spin diffusion and chemical exchange effects, which cannot be distinguished in a NOESY experiment for molecules the size of the globoside.

**Acknowledgment**. L.P. was a recipient of a fellowship from the Max-Planck-Gesellschaft. This work was supported by the Fritz Thyssen Stiftung (J.D.).

**Registry No.** Globotetraosylceramide, 11034-93-8.

**Supplementary Material Available:** Listing of cross-peak volumes obtained from 2D ROESY spectra recorded at different temperatures for solutions in $Me_2SO$-$d_6$ and $Me_2NCHO$-$d_7$ (4 pages). Ordering information is given on any current masthead page.

(51) Lipari, G.; Szabo, A. *J. Am. Chem. Soc.* **1982**, *104*, 4546–4570.
(52) Chachaty, C. *Prog. Nucl. Magn. Reson. Spectrosc.* **1987**, *19*, 183–222.
(53) Szabo, A. *Ann. N.Y. Acad. Sci.* **1986**, *482*, 44–50.
(54) Ha, S. N.; Giammona, A.; Field, M.; Brady, J. W. *Carbohydr. Res.* **1988**, *180*, 207–221.